Published in final edited form as:
Nanomedicine. 2013 August ; 9(6): 786–794. doi:10.1016/j.nano.2013.01.007.

Nanoparticle translocation across mouse alveolar epithelial cell monolayers: species-specific mechanisms

Farnoosh Fazlollahi, PhD[1,8], **Yong Ho Kim, PhD**[1,2], **Arnold Sipos, MD, PhD**[1,2], **Sarah F. Hamm-Alvarez, PhD**[6], **Zea Borok, MD**[1,2,3,±], **Kwang-Jin Kim, PhD**[1,2,5,6,7], and **Edward D. Crandall, PhD, MD**[1,2,4,8,*]

[1]Will Rogers Institute Pulmonary Research Center, University of Southern California, Los Angeles, CA, USA

[2]Department of Medicine, University of Southern California, Los Angeles, CA, USA

[3]Department of Biochemistry and Molecular Biology, University of Southern California, Los Angeles, CA, USA

[4]Department of Pathology, University of Southern California, Los Angeles, CA, USA

[5]Department of Physiology and Biophysics, University of Southern California, Los Angeles, CA, USA

[6]Department of Pharmacology and Pharmaceutical Sciences, University of Southern California, Los Angeles, CA, USA

[7]Department of Biomedical Engineering, University of Southern California, Los Angeles, CA, USA

[8]Mork Family Department of Chemical Engineering and Materials Science, University of Southern California, Los Angeles, CA, USA

Abstract

Studies of polystyrene nanoparticle (PNP) trafficking across mouse alveolar epithelial cell monolayers (MAECM) show apical-to-basolateral flux of 20 and 120 nm amidine-modified PNP is ~65 times faster than that of 20 and 100 nm carboxylate-modified PNP, respectively. Calcium chelation with EGTA has little effect on amidine-modified PNP flux but increases carboxylate-modified PNP flux ~50-fold. PNP flux is unaffected by methyl-β-cyclodextrin while ~70% decrease in amidine- (but not carboxylate-) modified PNP flux occurs across chlorpromazine- or dynasore-treated MAECM. Confocal microscopy reveals intracellular amidine- and carboxylate-modified PNP and association of amidine- (but not carboxylate-) modified PNP with clathrin heavy chain. These data indicate (1) amidine-modified PNP translocate across MAECM primarily via clathrin-mediated endocytosis and (2) physicochemical properties (e.g., surface charge) determine PNP interactions with mouse alveolar epithelium. Uptake/trafficking of nanoparticles into/across epithelial barriers are dependent on both nanoparticle physicochemical properties and (based on comparison with our prior results) specific epithelial cell type.

[*]To whom correspondence should be addressed: Edward D. Crandall, Ph.D., M.D., Department of Medicine, University of Southern California, IRD 606, 2020 Zonal Avenue, Los Angeles, CA 90033, USA, Office: 323 226-7593, Fax: 323 226-2899, ecrandal@usc.edu.
[±]Z. Borok is Ralph Edgington Chair in Medicine.
[*]E. D. Crandall is Hastings Professor and Kenneth T. Norris Jr. Chair of Medicine.

Keywords

epithelial transport; endocytosis; clathrin; dynamin; surface charge

Background

Inhalation of nanoparticles (NP; ≤ 100 nm at least in one dimension), including ambient ultrafine particles (i.e., overlapping size range with NP), are thought to be associated with cardiac arrhythmias, atherogenesis, clotting disorders and other health effects [1–3]. Inhaled NP have been found in liver, blood vessels, heart and other end organs [4–6]. The most likely route by which inhaled NP enter the systemic circulation is across the lung alveolar epithelium with its large surface area (~100 m^2 in human) and thin barrier thickness (~0.5 μm). Potential mechanisms for the pathophysiologic effects of inhaled NP remain largely speculative, but could include lung inflammation with subsequent effects on end organs and/or direct interactions of systemically circulating NP with end organs [7, 8]. Concerns about the health risks of NP [9–11], and interest in the use of NP for therapeutic applications [12–14], require better understanding of interactions (injury, uptake and trafficking) of inhaled NP with lung alveolar epithelium.

Distal airspaces of the lung are lined with alveolar epithelial type I (ATI) and type II (ATII) cells. ATI cells cover ~95% of the distal airspaces of the normal mammalian lung with extremely thin cytoplasmic extensions which are thought to facilitate efficient gas exchange and alveolar fluid homeostasis [15]. ATII cells also participate in alveolar fluid balance and secrete surfactants which enhance spreading of inhaled particles in alveolar airspaces [16–19]. ATII cells are known to undergo morphologic [19] and phenotypic [20] transition into ATI(-like) cells in primary culture. Due to the complex anatomy of the lung, specific mechanistic information pertaining to alveolar epithelial barrier properties and trafficking characteristics of macromolecules/NP is difficult to obtain from *in vivo* studies alone. Accordingly, alveolar epithelial cell monolayers in primary culture have been widely used [21, 22] as a representative *in vitro* model of the alveolar epithelial barrier. For example, we recently reported trafficking properties of polystyrene NP (PNP) with variable size and surface charge across primary cultured rat alveolar cell monolayers (RAECM) [23, 24]. In brief, translocation of 20–120 nm PNP across RAECM is dependent on both surface charge density and size, in that (a) flux is ~20–40 times greater for positively charged PNP than negatively charged PNP of similar size and (b) larger PNP (100 or 120 nm) cross RAECM ~3–4 times slower than smaller PNP (20 nm) with similar surface charge [24]. PNP appear to be translocated across RAECM via nonendocytic transcellular pathways, possibly involving diffusion across the lipid bilayer of cell plasma membranes [23].

In this study, primary cultured mouse alveolar epithelial cell monolayers (MAECM) were utilized to explore species-specific properties of PNP interactions with alveolar epithelium, especially in comparison to our prior findings with RAECM. Fluxes of amidine-modified (positively charged, 20 and 120 nm) PNP and carboxylate-modified (negatively charged, 20 and 100 nm) PNP were measured across MAECM in the presence and absence of inhibitors of endocytic (caveolin-, clathrin-, and dynamin-mediated) processes. Similarities and differences between PNP interactions with MAECM and our prior findings with RAECM were examined.

Methods

Nanoparticles

Fluorescently labeled polystyrene nanoparticles (PNP) were purchased from Thermo Fisher Scientific (Waltham, MA). Carboxylate-modified (COO^-, negatively charged, 20 and 100 nm diameter with surface charge of −304.3 and −320.0 μEq/g, respectively) and amidine-modified (HNC-NH_2^+, positively charged, 20 and 120 nm with surface charge of 80.2 and 39.7 μEq/g, respectively) PNP were used. Excitation/emission wavelengths for carboxylate- and amidine-modified PNP are 580/605 and 490/515 nm, respectively.

MAECM

Detailed descriptions for isolation of ATII cells from 129S6/SvEv mice (Taconic, Germantown, NY) and primary culture of mouse alveolar epithelial cells were recently published [25]. Handling of mice and *in vitro* procedures were approved by the University of Southern California Institutional Animal Care and Use Committee. In brief, after mice were anesthetized with pentobarbital sodium (400 mg/kg ip; Ovation Pharmaceuticals, Deerfield, IL), the abdominal cavity was opened and the animal exsanguinated. Lungs were perfused and lavaged *in situ* with phosphate-buffered saline (PBS, pH 7.4). Dispase (BD Bioscience, Bedford, MA) was instilled into lungs via the trachea (cannulated with a 20-gauge barrel-tip needle), followed by 0.5 mL of 1% low melting point agarose (Sigma, St. Louis, MO). Enzyme-treated lungs were excised and incubated with dispase for 45 min at room temperature. Lungs were dissected and chopped into a 1:1 mixture of Dulbecco's modified Eagle's medium and Ham's F-12 (DME/F-12; Sigma) supplemented with 0.01% DNase (Roche, Basel, Switzerland), 1 mM L-glutamine (Sigma), 10 mM N-(2-hydroxyethyl)piperazine-N′-(2-ethanesulfonic acid) (HEPES; Sigma), 0.1 mM nonessential amino acids (Sigma), and 0.2% Primocin (Invitrogen, San Diego, CA), followed by passage through a series of Nitex filters (100, 40, 20, and 10 μm; Tetko, Elmsford, NY). After centrifugation, macrophages and erythrocytes were removed from the crude cell mixture by incubation with biotinylated antibodies (anti-CD45, anti-Ter 119 and anti-CD16/32; BD Biosciences) diluted in medium containing 10% fetal bovine serum (FBS; Hyclone, Thermo Scientific, Rockford, IL), followed by positive selection with streptavidin-conjugated magnetic beads (Promega, Madison, WI). The partially purified cell mixture was incubated for 2 h at 37°C on Petri dishes precoated with mouse IgG (Sigma). Nonadherent alveolar epithelial cells were collected from IgG plates and resuspended in complete mouse medium (CMM), consisting of DMEM/F-12 supplemented with 1 mM L-glutamine, 0.1 mM nonessential amino acids, 10 mM HEPES, 0.25% bovine serum albumin (BSA; BD Bioscience), 0.05% insulin-transferrin-sodium selenite (Roche) and 0.2% Primocin. Tissue culture-treated polycarbonate filters (Transwell, 0.4 μm pore size, 1.13 cm^2, Corning Costar, Cambridge, MA) were precoated with 1 μg/mL laminin 5 (Chemicon, Billerica, MA) for 1 h at room temperature. Purified mouse ATII cells in CMM supplemented with 10% newborn bovine serum (Thermo Scientific) were plated onto these filters at 7.5×10^5 cells/cm^2. Cell culture medium was replaced with serum-free CMM 3 days after plating and every other day thereafter. Monolayers were maintained in a humidified 5% CO_2 + 95% air incubator at 37°C. A rapid screening device (Millicell-ERS; Millipore, Bedford, MA) was used to monitor transmonolayer resistance (Rt) and potential difference (PD) on day 3 in culture and onward. Confluent MAECM were studied on days 5–6 (Rt ~2 KΩ·cm^2 and PD ~10 mV).

Apical-to-basolateral PNP flux

To measure rates of PNP trafficking across MAECM, apical fluid was replaced at t = 0 with fresh culture medium containing various PNP. Apical-to-basolateral flux (J) of PNP at 37°C was estimated from PNP appearing in basolateral fluid over 24 h using SpectraMax M2 (Molecular Devices, Sunnyvale, CA). Apical [PNP] was determined at t = 0 and at the end

of flux measurements. We used an apical concentration of 176 μg/mL PNP to ensure reliable downstream fluorometric measurements for all PNP studied [24]. [PNP] was calculated using standard curves generated from known concentrations of PNP suspended in culture medium. Flux was calculated as $J = (CV)/S/\Delta t$, where C is [PNP] in basolateral fluid at Δt, V is basolateral fluid volume, S is nominal surface area of monolayer (1.13 cm^2) and Δt is length of time for flux measurement.

To determine if decreased tight junctional resistance leads to increased trafficking, flux of various PNP was measured in the presence of 2 mM EGTA (Sigma). Monolayers were pretreated with EGTA for 30 min, after which apical fluid was replaced at t = 0 with fresh culture medium containing various PNP at 176 μg/mL and 2 mM EGTA. During the flux measurements, 2 mM EGTA was present in both apical and basolateral fluids of MAECM. Bioelectric properties (i.e., PD and Rt) were monitored during EGTA experiments.

To explore mechanisms of PNP uptake into and translocation across MAECM, effects of inhibition of lipid raft-mediated (including caveolin-mediated) endocytosis were evaluated using methyl-β-cyclodextrin (MBC) [23, 26–29], chlorpromazine was employed for inhibition of clathrin-mediated endocytosis [23, 29, 30] and dynasore was used to inhibit dynamin-dependent (including both clathrin- and caveolin-mediated) endocytosis [23, 27, 29]. MAECM were bathed on both sides with culture medium containing 200 μM MBC (Sigma), 28 μM chlorpromazine (Sigma) or 80 μM dynasore (Sigma) for 30 min prior to replacing apical fluid at t = 0 with fresh culture medium containing both 176 μg/mL of various PNP and respective specific endocytosis inhibitors. During flux measurements, the endocytosis inhibitor was present in both apical and basolateral fluids of MAECM. As positive control, flux of FITC-cholera toxin subunit B (CTB; Sigma), which in many cell types has been shown to be transported via caveolin-mediated endocytosis [23], was measured at 2 h in the presence or absence of 200 μM MBC with an apical [CTB] of 50 μg/mL.

Immunofluorescence and confocal laser scanning microscopy (CLSM)

MAECM were exposed apically to 176 μg/mL amidine-modified (positively charged, 120 nm) or carboxylate-modified (negatively charged, 100 nm) PNP at 37°C for 24 h. Exposed monolayers were washed 3 times with ice-cold PBS (pH 7.2) and fixed in 3.7% formaldehyde (J.T. Baker, Phillipsburg, NJ) at room temperature for 15 min. Fixed monolayers were permeabilized with 0.5% Triton X-100 (TX-100, Bio-Rad, Hercules, CA) for 15 min at room temperature, followed by rinsing with PBS and blocking with 5% BSA and 0.2% TX-100 in PBS for 1 h at room temperature. Blocked monolayers were incubated with a rabbit antibody against zonula occludens-1 (ZO-1, Zymed Laboratories, San Francisco, CA) diluted (1:100) with 1% BSA in PBS for 1 h at 37°C. Monolayers were then incubated with a goat anti-rabbit antibody conjugated to Alexa 594 or Alexa 488 (Invitrogen) diluted 1:100 with 1% BSA in PBS at 37°C for 1 h, rinsed with PBS and mounted on microscope slides with mounting medium (containing the nuclear staining dye 4',6-diamidino-2-phenylindole (DAPI) (Vector, Burlingame, CA)). Distributions of PNP in MAECM were acquired with a Zeiss confocal laser scanning microscope (510 Meta NLO CLSM imaging system, Jena, Germany) equipped with argon and red/green HeNe lasers mounted on a vibration-free table and attached to an incubation chamber.

In some experiments, MAECM were pretreated with EGTA (2 mM) for 30 min prior to apical exposure for 24 h to amidine-modified (positively charged, 120 nm) or carboxylate-modified (negatively charged, 100 nm) PNP at 176 μg/mL in the presence of both apical and basolateral 2 mM EGTA, followed by CLSM. These EGTA-treated and PNP-exposed MAECM were processed as above for non-EGTA treated and PNP-exposed MAECM. Distributions of PNP in these EGTA-treated MAECM were studied by CLSM as above.

To determine if PNP colocalize with clathrin heavy chain, MAECM exposed apically to amidine-modified (positively charged, 120 nm) or carboxylate-modified (negatively charged, 100 nm) PNP at 176 μg/mL for 2 h were fixed and permeabilized with ice-cold ethanol at −20°C for 5 min. Monolayers were then blocked with 5% BSA and 0.2% TX-100 in PBS at room temperature for 1 h. Blocked monolayers were incubated with mouse antibody against human clathrin heavy chain (BD Biosciences) diluted 1:100 with 1% BSA in PBS for 1 h at 37°C, washed thrice with PBS, and incubated with a secondary antibody (goat anti-mouse antibody labeled with Alexa 488 or Alexa 594) diluted 1:100 with 1% BSA in PBS for 1 h at 37°C. Monolayers were then rinsed with PBS and mounted on microscope slides with mounting medium containing DAPI. Colocalization of PNP with clathrin heavy chain was studied by CLSM as above. As negative controls, monolayers not exposed to PNP or those incubated only with a primary or secondary antibody were similarly processed and imaged by CLSM.

Data analysis

Data are presented as mean ± standard error (n = total number of MAECM). Unpaired Student's *t*-tests were performed for comparisons of two group means. One-way analysis of variance followed by post-hoc tests based on modified Newman-Keuls procedures was performed to determine differences among means of ≥3 groups. $P<0.05$ was considered statistically significant.

Results

Figure 1 shows flux of amidine-modified (positively charged, 20 and 120 nm) and carboxylate-modified (negatively charged, 20 and 100 nm) PNP across MAECM with apical [PNP] of 176 μg/mL. Trafficking of 20 and 100 nm negatively charged PNP are not significantly different. Trafficking of 20 and 120 nm positively charged PNP are also not significantly different, but each is ~65 times faster than trafficking of 20 and 100 nm negatively charged PNP.

Rt of MAECM decreased >95% in the presence of 2 mM EGTA (which chelates free Ca^{2+}) in both apical and basolateral fluids. Flux of amidine-modified PNP (positively charged, 20 and 120 nm) across MAECM was not significantly changed in the presence of EGTA, while flux of 20 and 100 nm carboxylate-modified PNP across MAECM was markedly increased by ~60 and ~40 fold, respectively (Figure 2).

Figure 3 shows flux of amidine-modified PNP (positively charged, 20 and 120 nm) in the presence and absence of 200 μM MBC, 28 μM chlorpromazine or 80 μM dynasore. No decrease was seen in flux of positively or negatively charged PNP in the presence of 200 μM MBC, as depicted in Figure 3 and Supplementary Table S1. In contrast, flux of CTB (positive control) decreased ~98% (from control flux of 20.72 ± 3.06 (n=6) pg/s/cm^2) in the presence of MBC (Figure 3). Rt of MAECM treated with MBC decreased ~5% compared to that of control monolayers. In contrast, flux of amidine-modified (positively charged, 20 and 120 nm) PNP decreased ~60–80% in the presence of chlorpromazine or dynasore compared to respective controls. Fluxes of carboxylate-modified (negatively charged, 20 and 100 nm) PNP did not decrease in the presence of chlorpromazine or dynasore (Supplementary Table S1), while Rt of MAECM treated with chlorpromazine or dynasore decreased ~30% compared to that of control monolayers.

Confocal photomicrographs of MAECM exposed apically to 176 μg/mL PNP (amidine-(positively charged) 120 nm or carboxylate-modified (negatively charged) 100 nm) for 24 h are shown in Figure 4A–B. Both negatively and positively charged PNP are observed intracellularly.

Figures 5A–B show confocal micrographs of MAECM exposed to 176 μg/mL PNP (120 nm amidine-modified (positively charged) and 100 nm carboxylate-modified (negatively charged)) in the presence of 2 mM EGTA after 24 h. Association of a few carboxylate (but not amidine)-modified PNP with cell-cell junctions of MAECM treated with EGTA may be seen (arrows in panel B).

Figure 6A shows intracellular amidine-modified PNP (positively charged, 120 nm) and clathrin heavy chain after 1 h exposure of MAECM to apical [PNP] of 176 μg/mL. Along the profiling path marked with the white arrow (Figure 6A), corresponding intensity profiles for both PNP (green curve in Figure 6B) and clathrin heavy chain (red curve in Figure 6B) using CLSM software were generated. These data, while consistent with intracellular co-localization of PNP and clathrin, are not conclusive because of the diffuse nature of cytoplasmic clathrin fluorescence.

Discussion

This study demonstrates that translocation of PNP across MAECM under baseline conditions occurs transcellularly in a manner strongly dependent on nanoparticle surface charge. Moreover, positively (but not negatively) charged PNP traverse MAECM via a clathrin-mediated pathway. Strikingly, decreasing tight junctional resistance of MAECM with calcium chelation causes drastic increases in paracellular translocation of negatively (but not positively) charged PNP. As discussed further below, comparison with our prior reports on PNP trafficking across RAECM [23, 24] and Madin Darby canine kidney epithelial cell monolayers (MDCK-II) [27] suggests that mechanisms of PNP trafficking across epithelial barriers is highly cell type- and species-dependent.

We previously reported that cationic PNP (amidine-modified (positively charged)) are translocated ~40 and ~500 times faster than anionic PNP (carboxylate-modified (negatively charged)) across RAECM and MDCK-II, respectively [24, 27]. In this study, trafficking of amidine-modified (positively charged) PNP across MAECM has been shown to be ~65 times faster than that of carboxylate-modified (negatively charged) PNP of similar size (Figure 1). It can be noted that aggregation status of nanoparticles during the 24 h period of apical exposure could impact flux measurements, although the observed differences in flux of positively charged PNP vs negatively charged PNP are clearly due to charge (and in part size) as shown in this and prior studies [24, 27]. The degree of aggregation, assessed by dynamic light scattering, for amidinated PNP is greater than that for carboxylated PNP (data not shown), indicating that surface charge is the predominant factor in observed rates of PNP translocation across MAECM.

In addition to charge-mediated interactions with cell surface glycocalyx [31, 32], hydrophobicity of particles may play a role in their cellular interactions and subsequent trafficking. It has been reported that amidine-modified (positively charged) polystyrene particles (200 nm) have higher hydrophobicity and translocate faster across intestinal epithelial (Caco-2) cell monolayers than similarly sized carboxylate-modified (negatively charged) polystyrene particles [33]. Our laboratory also reported that amidine-modified PNP are more hydrophobic than carboxylate-modified (negatively charged) PNP [23], which may contribute to more rapid diffusion of amidine-modified (positively charged) PNP through lipid bilayers of cell plasma membranes and/or promote PNP interactions with cell membrane components (e.g., coated pits; see below).

Trafficking of 20 nm amidine-modified (positively charged) PNP is not significantly different from 120 nm amidine-modified PNP across MAECM (Figure 1). Similar flux profiles were observed for carboxylate-modified (negatively charged) PNP of 20 and 100

nm. We previously reported absence of size dependency in translocation of PNP of similar surface charge across MDCK-II as well [27]. Conversely, we reported that smaller PNP (20 nm) translocate across RAECM ~3 times faster than larger PNP (100 or 120nm) with similar charge [24]. Dos Santos et al [34] studied uptake of carboxyl-modified PNP (40–2000 nm) using various cell lines, including human glial astrocytoma (1321N1), murine macrophage-like cells (RAW 264.7), human cervix epithelial cells (HeLa), human lung epithelial cells (A549) and human brain capillary endothelial cells (HCMEC D3) and reported that, within a given cell line, uptake of larger PNP is much slower than that of smaller PNP.

Treatment of epithelial cells with EGTA (calcium chelator) increases paracellular permeability to ions and hydrophilic solutes by changing the distribution of a number of adherens junctional/cytoskeletal proteins [35–38]. Trafficking of positively charged PNP (20 and 120 nm) across MAECM in the presence of 2 mM EGTA did not change significantly compared to respective controls, while trafficking of negatively charged PNP (20 and 100 nm) across MAECM in the presence of 2 mM EGTA increased by ~60 and ~40 fold, respectively (Figure 2). This latter observation could be due in part to the greater hydrophobicity of positively charged PNP compared to negatively charged PNP, leading to exclusion of positively charged PNP from disrupted paracellular pathways and/or EGTA-associated augmentation of the charge-selective properties of tight junctions (i.e., favoring movement of negatively charged substances through tight junctions). This result indicates that positively charged (but not negatively charged) PNP do not traverse MAECM via tight junctional pathways at baseline or following EGTA treatment. These findings, along with localization of positively charged PNP exclusively inside cells while some negatively charged PNP can be seen at cell-cell junctions in the presence of EGTA (Figures 5A and 5B), indicate that negatively charged (but not positively charged) PNP may cross EGTA-treated MAECM in part via paracellular pathways. EGTA treatment may also have activated/upregulated other pathways (e.g., endocytic pathways which at baseline do not participate in cellular uptake of negatively (but not positively) charged PNP). When Yacobi et al [23] applied the same experimental approach, it was found that translocation of both positively and negatively charged PNP across RAECM takes place predominantly via non-endocytic transcellular pathways. We also recently showed that PEGylated quantum dots (core size ~5 nm, hydrodynamic size ~25 nm, amine-, carboxylate- and non-modified) can traverse EGTA-disrupted tight junctions [29].

Lipid raft-mediated endocytosis (including caveolin-mediated endocytosis, CLIC/GEEC endocytosis, arf6-mediated endocytosis, flotillin-mediated endocytosis and macropinocytosis) can be disrupted when plasma membrane cholesterol is decreased [26, 30]. ATI cells are richly endowed with caveolae [39]. One of the ways to disrupt caveolae formation is to extract cholesterol from cell membranes (e.g., using MBC, a sterol-binding drug that sequesters cholesterol and inhibits formation of lipid rafts). As seen, 200 μM MBC markedly decreases flux of CTB, while PNP (carboxylate (negatively charged, 20 and 100 nm)- or amidine (positively charged, 20 and 120 nm)-modified) flux across MAECM did not decrease (Figure 3), suggesting that translocation of PNP across MAECM does not take place via lipid raft-mediated endocytosis. Dausend et al [40] reported that cholesterol depletion did not decrease positively (113 nm) or negatively (121 nm) charged PNP uptake into HeLa cells. In addition, our laboratory has recently reported that translocation of PNP (positively and negatively charged) across RAECM or MDCK-II was not decreased in the presence of 200 μM MBC [23, 27], suggesting that PNP are not taken up into cells via lipid raft-mediated endocytosis in these two epithelial barriers.

Involvement of clathrin-mediated endocytosis in uptake/translocation of various NP in cells and tissues has been reported. For example, uptake of positively charged PNP into MDCK-II cells [27], cationic polysaccharide NP prepared from maltodextrin into airway epithelial

cells [41], PEGylated D,L-polylactide (PEG-PLA) NP into HeLa cells [42] and fullerenic NP into rat fibroblasts and rat hepatoma cells [43] all were reported to take place via clathrin-mediated endocytosis. The assembly unit of clathrin, triskelion, is a three-legged structure comprised of three heavy and three light chains. Assembly of the triskelion leads to formation of a net-like basket (clathrin-coated pit) at the cell plasma membrane. The maximum diameter of clathrin-coated pits is ~100–150 nm [40]. The most abundant proteins found in clathrin-coated pits are clathrin and the heterotetrameric adaptor protein 2 (AP-2) [44]. Chlorpromazine causes clathrin and AP-2 to relocate to multivesicular bodies, causing inhibition of clathrin-mediated endocytosis [23, 29]. Treatment of MAECM with 28 μM chlorpromazine in this study led to ~60–80% decrease in trafficking of amidine-modified (positively charged, 20 and 120 nm) but not carboxylate-modified (negatively charged, 20 and 100 nm) PNP (Figure 3), consistent with the notion that positively (but not negatively) charged NP preferentially associate with clathrin-coated pits and are subsequently taken up into/translocated across certain (but not all) epithelial barriers.

Charge-dependent clathrin-mediated uptake of positively (but not negatively) charged PEG-PLA NP into HeLa and MDCK-II cells has been reported [42, 45]. Recently, our laboratory also reported charge-dependent clathrin-mediated endocytosis of positively charged (but not negatively charged) PNP (20 and 120 nm) across MDCK-II [27]. In this regard, our data on greater trafficking of positively charged (compared to negatively charged) PNP across MAECM may be governed by a similar charge-dependence of clathrin-mediated endocytosis. However, clathrin-mediated trafficking of positively charged PNP across epithelial barriers appears to be cell- and/or species-specific, since trafficking of the same PNP (i.e., 20–120 nm, amidinated or carboxylated) across RAECM does not appear to take place via clathrin-mediated endocytosis [23]. Importantly, flux across MAECM of transferrin (at an apical concentration of 500 μg/mL), known to be taken up into epithelial cells via clathrin-mediated endocytosis [23, 46], is ~3 times greater than that across RAECM (Supplementary Information, Figure S1), consistent with the possibility that the difference in the predominant mechanism(s) of amidinated PNP translocation across RAECM vs MAECM is due in part to the different capacities for clathrin-mediated transcytosis in these two epithelial barriers.

The membrane scission protein dynamin is a large GTPase which forms a helical polymer around the constricted neck of newly formed cell plasma membrane invaginations and, upon GTP hydrolysis, mediates fission of the vesicle from the plasma membrane. Dynamin is essential for formation of caveolin- and clathrin-coated vesicles and is involved in some other lipid raft-mediated processes [26]. Dynasore is a small cell-permeable molecule that acts as a selective non-competitive inhibitor of the GTPase protein dynamin. This inhibitor has been shown to block dynamin-dependent endocytosis by inhibiting dynamin GTPase and thus blocking formation of intracellular vesicle liberation from cell membranes [47]. Our data showing that the presence of 80 μM dynasore decreases trafficking of positively charged PNP across MAECM most likely reflect decreased trafficking via clathrin-mediated pathways, since caveolae-mediated process(es) do not appear to be involved (Figure 3). We reported recently that dynasore decreases trafficking of 20 and 120 nm positively charged (but not 20 and 100 nm negatively charged) PNP across MDCK-II [27]. We also reported that dynasore has no effect on trafficking of the same positively or negatively charged PNP across RAECM, indicating that PNP trafficking across RAECM does not take place via endocytosis that requires dynamin activity [23].

These findings obtained using *in vitro* models may not directly correlate with *in vivo* trafficking of PNP due to the presence of other factors in the lungs of live animals. Interactions of inhaled/instilled nanoparticles with lung resident macrophages (and other blood-borne cells) and/or alveolar fluid components (e.g., surfactant) may play important

role(s) in the fate of inhaled/instilled nanoparticles. It has been reported that alveolar macrophages can phagocytose nanoparticles (e.g., iridium, and gold) [6, 48]. Surfactant may modify the surface properties of inhaled/instilled nanoparticles which reach the alveoli [49, 50]. Interestingly, we found that serum in culture media did not significantly affect charge-dependent trafficking of PNP across RAECM (unpublished observations), suggesting that modification of PNP did not lead to major alterations in mechanisms underlying PNP translocation across RAECM. Correlation of *in vitro* and *in vivo* findings of PNP-alveolar epithelial interactions will require further *in vivo* studies.

In summary, we have shown that translocation of amidine-modified (positively charged, 20 and 120 nm) PNP across MAECM occurs transcellularly and involves clathrin/dynamin-dependent endocytosis. Translocation of carboxylate-modified (negatively charged) 20 and 100 nm PNP across MAECM likely occurs both transcellularly (via non-endocytic pathways) and paracellularly. Greater trafficking of amidine-modified (positively charged) PNP compared to that of carboxylate-modified (negatively charged) PNP of similar size across MAECM may be related primarily to the charge-selective behavior of clathrin-mediated endocytosis. Since PNP do not traverse RAECM via endocytic mechanisms [23, 24], we conclude that nanoparticle interactions with epithelial barriers are both nanoparticle physicochemical property (e.g., surface charge and size)- and epithelial cell type-specific.

Supplementary Material

Refer to Web version on PubMed Central for supplementary material.

Acknowledgments

Contract grant sponsor: Hastings Foundation, Whittier Foundation and National Institutes of Health Research Grants: ES017034, ES018782, EY011386, EY017923, HL038621, HL062569 and HL089445.

The authors appreciate the technical assistance of Mr. Juan Raymond Alvarez.

References

1. Mills NL, Donaldson K, Hadoke PW, Boon NA, MacNee W, Cassee FR, et al. Adverse cardiovascular effects of air pollution. Nat Clin Pract Cardiovasc Med. 2009; 6:36–44. [PubMed: 19029991]
2. Brook RD, Franklin B, Cascio W, Hong Y, Howard G, Lipsett M, et al. Air pollution and cardiovascular disease: a statement for healthcare professionals from the Expert Panel on Population and Prevention Science of the American Heart Association. Circulation. 2004; 109:2655–2671. [PubMed: 15173049]
3. Araujo JA, Barajas B, Kleinman M, Wang X, Bennett BJ, Gong KW, et al. Ambient particulate pollutants in the ultrafine range promote early atherosclerosis and systemic oxidative stress. Circ Res. 2008; 102:589–596. [PubMed: 18202315]
4. Takenaka S, Karg E, Kreyling WG, Lentner B, Moller W, Behnke-Semmler M, et al. Distribution pattern of inhaled ultrafine gold particles in the rat lung. Inhal Toxicol. 2006; 18:733–740. [PubMed: 16774862]
5. Shimada A, Kawamura N, Okajima M, Kaewamatawong T, Inoue H, Morita T. Translocation pathway of the intratracheally instilled ultrafine particles from the lung into the blood circulation in the mouse. Toxicol Pathol. 2006; 34:949–957. [PubMed: 17178695]
6. Kreyling WG, Semmler-Behnke M, Seitz J, Scymczak W, Wenk A, Mayer P, et al. Size dependence of the translocation of inhaled iridium and carbon nanoparticle aggregates from the lung of rats to the blood and secondary target organs. Inhal Toxicol. 2009; 21(Suppl 1):55–60. [PubMed: 19558234]

7. Ho M, Wu KY, Chein HM, Chen LC, Cheng TJ. Pulmonary toxicity of inhaled nanoscale and fine zinc oxide particles: Mass and surface area as an exposure metric. Inhal Toxicol. 23:947–956. [PubMed: 22122307]
8. Kim JS, Adamcakova-Dodd A, O'Shaughnessy PT, Grassian VH, Thorne PS. Effects of copper nanoparticle exposure on host defense in a murine pulmonary infection model. Part Fibre Toxicol. 2011; 8:29–43. [PubMed: 21943386]
9. Oberdorster G, Oberdorster E, Oberdorster J. Nanotoxicology: an emerging discipline evolving from studies of ultrafine particles. Environ Health Perspect. 2005; 113:823–839. [PubMed: 16002369]
10. Peters A, Veronesi B, Calderon-Garciduenas L, Gehr P, Chen LC, Geiser M, et al. Translocation and potential neurological effects of fine and ultrafine particles a critical update. Part Fibre Toxicol. 2006; 3:13–26. [PubMed: 16961926]
11. LeBlanc AJ, Moseley AM, Chen BT, Frazer D, Castranova V, Nurkiewicz TR. Nanoparticle inhalation impairs coronary microvascular reactivity via a local reactive oxygen species-dependent mechanism. Cardiovasc Toxicol. 2010; 10:27–36. [PubMed: 20033351]
12. Cuenca AG, Jiang H, Hochwald SN, Delano M, Cance WG, Grobmyer SR. Emerging implications of nanotechnology on cancer diagnostics and therapeutics. Cancer. 2006; 107:459–466. [PubMed: 16795065]
13. Farokhzad OC, Langer R. Impact of nanotechnology on drug delivery. ACS Nano. 2009; 3:16–20. [PubMed: 19206243]
14. De Jong WH, Borm PJ. Drug delivery and nanoparticles: applications and hazards. Int J Nanomedicine. 2008; 3:133–149. [PubMed: 18686775]
15. Haefeli-Bleuer B, Weibel ER. Morphometry of the human pulmonary acinus. Anat Rec. 1988; 220:401–414. [PubMed: 3382030]
16. Fehrenbach H. Alveolar epithelial type II cell: defender of the alveolus revisited. Respir Res. 2001; 2:33–46. [PubMed: 11686863]
17. Crandall ED, Matthay MA. Alveolar epithelial transport. Basic science to clinical medicine. Am J Respir Crit Care Med. 2001; 163:1021–1029. [PubMed: 11282783]
18. Cheek JM, Kim KJ, Crandall ED. Tight monolayers of rat alveolar epithelial cells: bioelectric properties and active sodium transport. Am J Physiol. 1989; 256:C688–C693. [PubMed: 2923201]
19. Cheek JM, Evans MJ, Crandall ED. Type I cell-like morphology in tight alveolar epithelial monolayers. Exp Cell Res. 1989; 184:375–387. [PubMed: 2806398]
20. Danto SI, Zabski SM, Crandall ED. Reactivity of alveolar epithelial cells in primary culture with type I cell monoclonal antibodies. Am J Respir Cell Mol Biol. 1992; 6:296–306. [PubMed: 1540393]
21. Steimer A, Franke H, Haltner-Ukomado E, Laue M, Ehrhardt C, Lehr CM. Monolayers of porcine alveolar epithelial cells in primary culture as an in vitro model for drug absorption studies. Eur J Pharm Biopharm. 2007; 66:372–382. [PubMed: 17267190]
22. Geiser M, Rothen-Rutishauser B, Kapp N, Schurch S, Kreyling W, Schulz H, et al. Ultrafine particles cross cellular membranes by nonphagocytic mechanisms in lungs and in cultured cells. Environ Health Perspect. 2005; 113:1555–1560. [PubMed: 16263511]
23. Yacobi NR, Malmstadt N, Fazlollahi F, DeMaio L, Marchelletta R, Hamm-Alvarez SF, et al. Mechanisms of alveolar epithelial translocation of a defined population of nanoparticles. Am J Respir Cell Mol Biol. 2010; 42:604–614. [PubMed: 19574531]
24. Yacobi NR, Demaio L, Xie J, Hamm-Alvarez SF, Borok Z, Kim KJ, et al. Polystyrene nanoparticle trafficking across alveolar epithelium. Nanomedicine. 2008; 4:139–145. [PubMed: 18375191]
25. Demaio L, Tseng W, Balverde Z, Alvarez JR, Kim KJ, Kelley DG, et al. Characterization of mouse alveolar epithelial cell monolayers. Am J Physiol Lung Cell Mol Physiol. 2009; 296:L1051–L1058. [PubMed: 19329539]
26. Doherty GJ, McMahon HT. Mechanisms of endocytosis. Annu Rev Biochem. 2009; 78:857–902. [PubMed: 19317650]
27. Fazlollahi F, Angelow S, Yacobi NR, Marchelletta R, Yu AS, Hamm-Alvarez SF, et al. Polystyrene nanoparticle trafficking across MDCK-II. Nanomedicine. 2011; 7:588–594. [PubMed: 21310266]

28. Parton RG, Richards AA. Lipid rafts and caveolae as portals for endocytosis: new insights and common mechanisms. Traffic. 2003; 4:724–738. [PubMed: 14617356]
29. Fazlollahi F, Sipos A, Kim YH, Hamm-Alvarez SF, Borok Z, Kim KJ, et al. Translocation of PEGylated quantum dots across rat alveolar epithelial cell monolayers. Int J Nanomedicine. 2011; 6:2849–2857. [PubMed: 22131830]
30. Ivanov AI. Pharmacological inhibition of endocytic pathways: is it specific enough to be useful? Methods Mol Biol. 2008; 440:15–33. [PubMed: 18369934]
31. Martins Mde F, Bairos VA. Glycocalyx of lung epithelial cells. Int Rev Cytol. 2002; 216:131–173. [PubMed: 12049207]
32. DeFouw DO. Ultrastructural features of alveolar epithelial transport. Am Rev Respir Dis. 1983; 127:S9–S13. [PubMed: 6846951]
33. des Rieux A, Ragnarsson EG, Gullberg E, Preat V, Schneider YJ, Artursson P. Transport of nanoparticles across an in vitro model of the human intestinal follicle associated epithelium. Eur J Pharm Sci. 2005; 25:455–465. [PubMed: 15946828]
34. Dos Santos T, Varela J, Lynch I, Salvati A, Dawson KA. Quantitative assessment of the comparative nanoparticle-uptake efficiency of a range of cell lines. Small. 2011; 7:3341–3349. [PubMed: 22009913]
35. Collares-Buzato CB, McEwan GT, Jepson MA, Simmons NL, Hirst BH. Paracellular barrier and junctional protein distribution depend on basolateral extracellular Ca^{2+} in cultured epithelia. Biochim Biophys Acta. 1994; 1222:147–158. [PubMed: 8031850]
36. Knipp GT, Ho NF, Barsuhn CL, Borchardt RT. Paracellular diffusion in Caco-2 cell monolayers: effect of perturbation on the transport of hydrophilic compounds that vary in charge and size. J Pharm Sci. 1997; 86:1105–1110. [PubMed: 9344165]
37. Mounier J, Vasselon T, Hellio R, Lesourd M, Sansonetti PJ. Shigella flexneri enters human colonic Caco-2 epithelial cells through the basolateral pole. Infect Immun. 1992; 60:237–248. [PubMed: 1729185]
38. Sergent T, Parys M, Garsou S, Pussemier L, Schneider YJ, Larondelle Y. Deoxynivalenol transport across human intestinal Caco-2 cells and its effects on cellular metabolism at realistic intestinal concentrations. Toxicol Lett. 2006; 164:167–176. [PubMed: 16442754]
39. Newman GR, Campbell L, von Ruhland C, Jasani B, Gumbleton M. Caveolin and its cellular and subcellular immunolocalisation in lung alveolar epithelium: implications for alveolar epithelial type I cell function. Cell Tissue Res. 1999; 295:111–120. [PubMed: 9931357]
40. Dausend J, Musyanovych A, Dass M, Walther P, Schrezenmeier H, Landfester K, et al. Uptake mechanism of oppositely charged fluorescent nanoparticles in HeLa cells. Macromol Biosci. 2008; 8:1135–1143. [PubMed: 18698581]
41. Dombu CY, Kroubi M, Zibouche R, Matran R, Betbeder D. Characterization of endocytosis and exocytosis of cationic nanoparticles in airway epithelium cells. Nanotechnology. 2010; 21:355102–355110. [PubMed: 20689164]
42. Harush-Frenkel O, Debotton N, Benita S, Altschuler Y. Targeting of nanoparticles to the clathrin-mediated endocytic pathway. Biochem Biophys Res Commun. 2007; 353:26–32. [PubMed: 17184736]
43. Li W, Chen C, Ye C, Wei T, Zhao Y, Lao F, et al. The translocation of fullerenic nanoparticles into lysosome via the pathway of clathrin-mediated endocytosis. Nanotechnology. 2008; 19:145102–145114. [PubMed: 21817752]
44. Mousavi SA, Malerod L, Berg T, Kjeken R. Clathrin-dependent endocytosis. Biochem J. 2004; 377:1–16. [PubMed: 14505490]
45. Harush-Frenkel O, Rozentur E, Benita S, Altschuler Y. Surface charge of nanoparticles determines their endocytic and transcytotic pathway in polarized MDCK cells. Biomacromolecules. 2008; 9:435–443. [PubMed: 18189360]
46. Chen B, Liu Q, Zhang Y, Xu L, Fang X. Transmembrane delivery of the cell-penetrating peptide conjugated semiconductor quantum dots. Langmuir. 2008; 24:11866–11871. [PubMed: 18823093]
47. Macia E, Ehrlich M, Massol R, Boucrot E, Brunner C, Kirchhausen T. Dynasore, a cellpermeable inhibitor of dynamin. Dev Cell. 2006; 10:839–850. [PubMed: 16740485]

48. Sadauskas E, Jacobsen NR, Danscher G, Stoltenberg M, Vogel U, Larsen A, et al. Biodistribution of gold nanoparticles in mouse lung following intratracheal instillation. Chem Cent J. 2009; 3:16. [PubMed: 19930546]

49. Schleh C, Rothen-Rutishauser B, Kreyling WG. The influence of pulmonary surfactant on nanoparticulate drug delivery systems. Eur J Pharm Biopharm. 2011; 77:350–352. [PubMed: 21195761]

50. Kumar P, Bohidar HB. Interaction of soot derived multi-carbon nanoparticles with lung surfactants and their possible internalization inside alveolar cavity. Indian J Exp Biol. 2010; 48:1037–1042. [PubMed: 21299046]

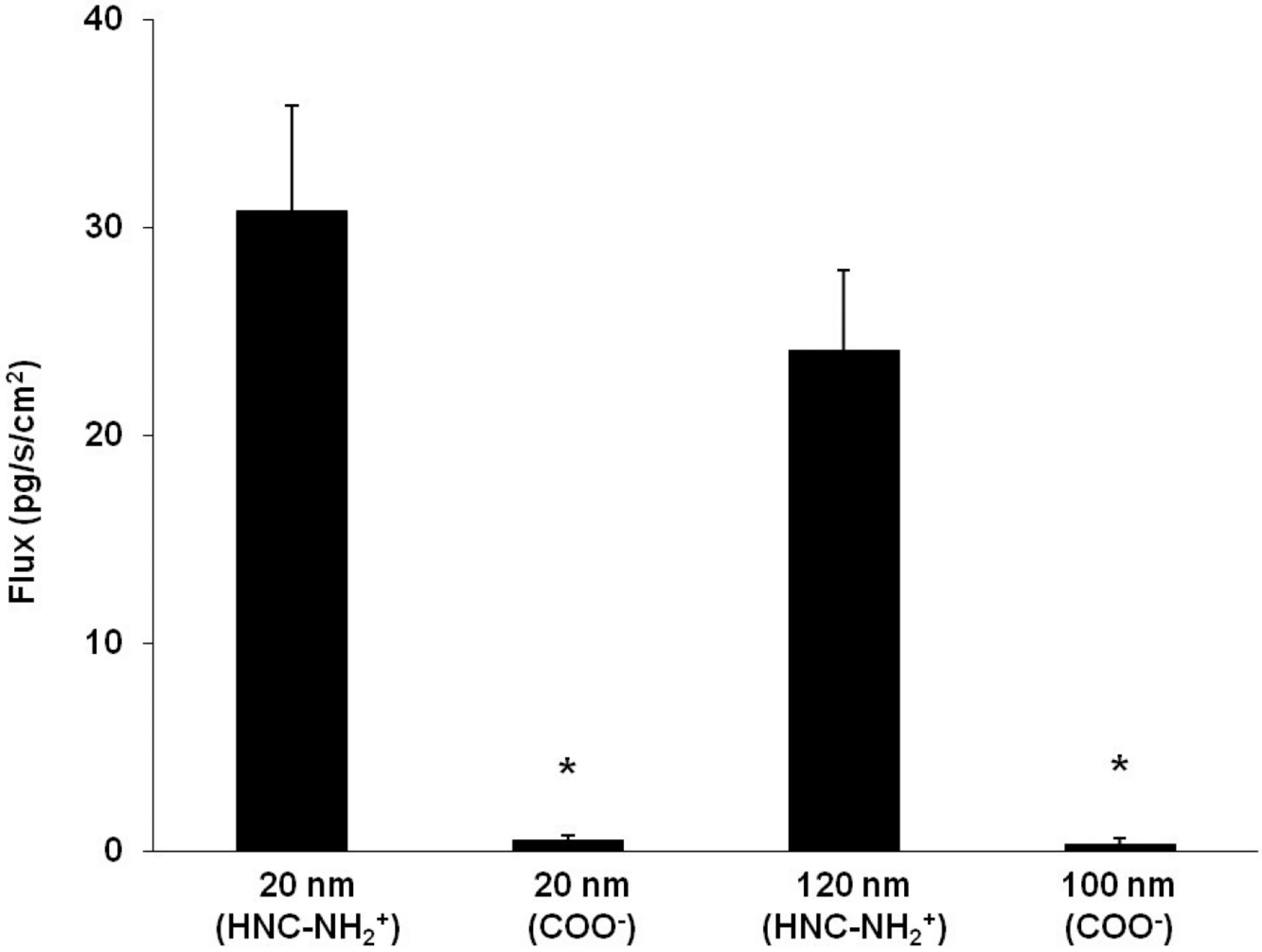

Figure 1.
Flux of PNP (amidine-modified (positively charged) 20 and 120 nm and carboxylate-modified (negatively charged) 20 and 100 nm) across MAECM at apical [PNP] of 176 μg/mL measured at 24 h (n=6). * = significantly different from flux of 20 and 120 nm amidine-modified (positively charged) PNP, respectively.

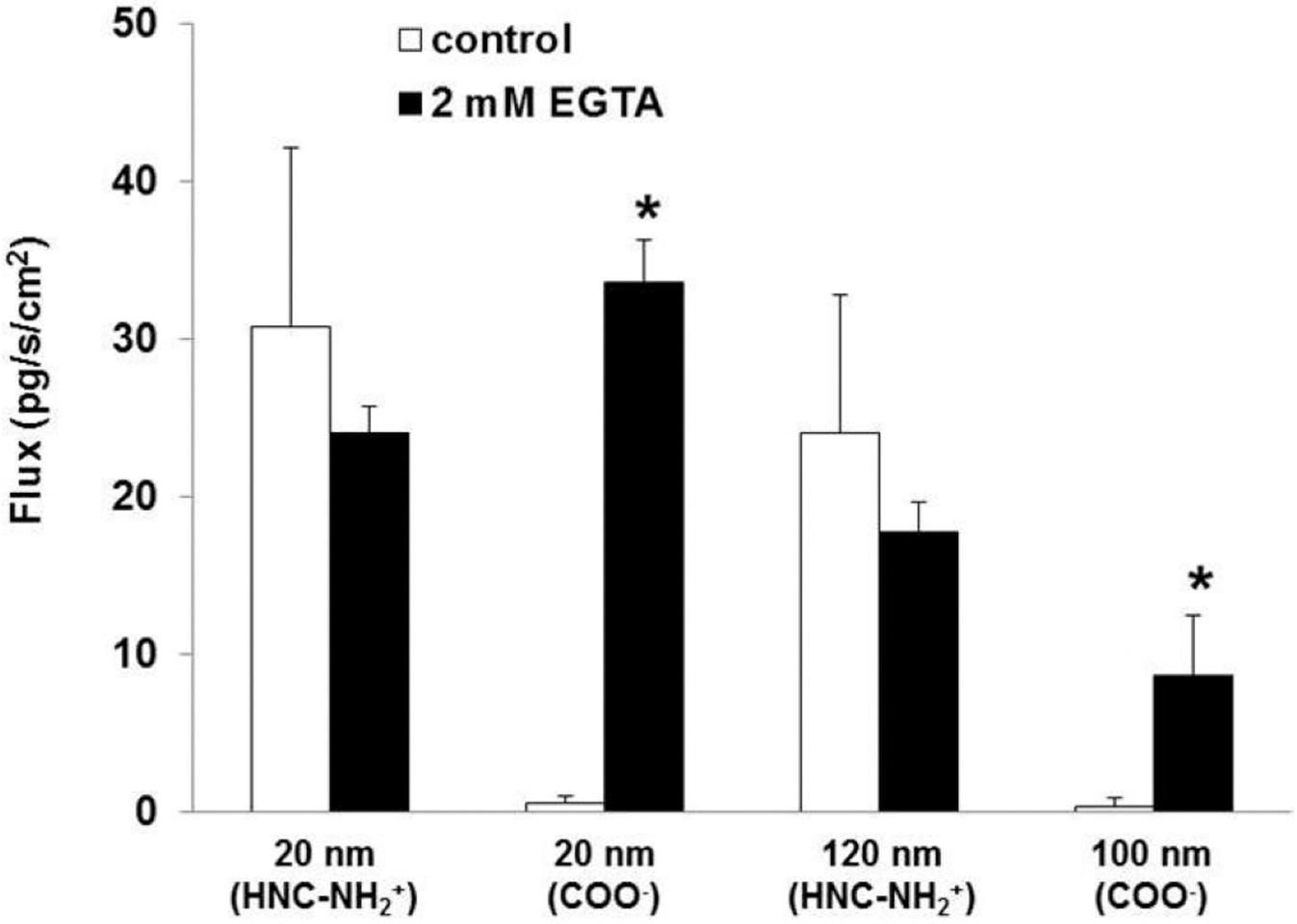

Figure 2.

Effects of 2 mM EGTA in both apical and basolateral bathing fluids on flux of PNP (amidine-modified (positively charged) 20 and 120 nm and carboxylate-modified (negatively charged) 20 and 100 nm) assessed at 24 h across MAECM at apical [PNP] of 176 μg/mL. Flux of amidine-modified (positively charged) PNP did not increase in the presence of 2 mM EGTA, while flux of carboxylate-modified (negatively charged) PNP increased significantly in the presence of 2 mM EGTA (n=5). * = significantly different from respective control.

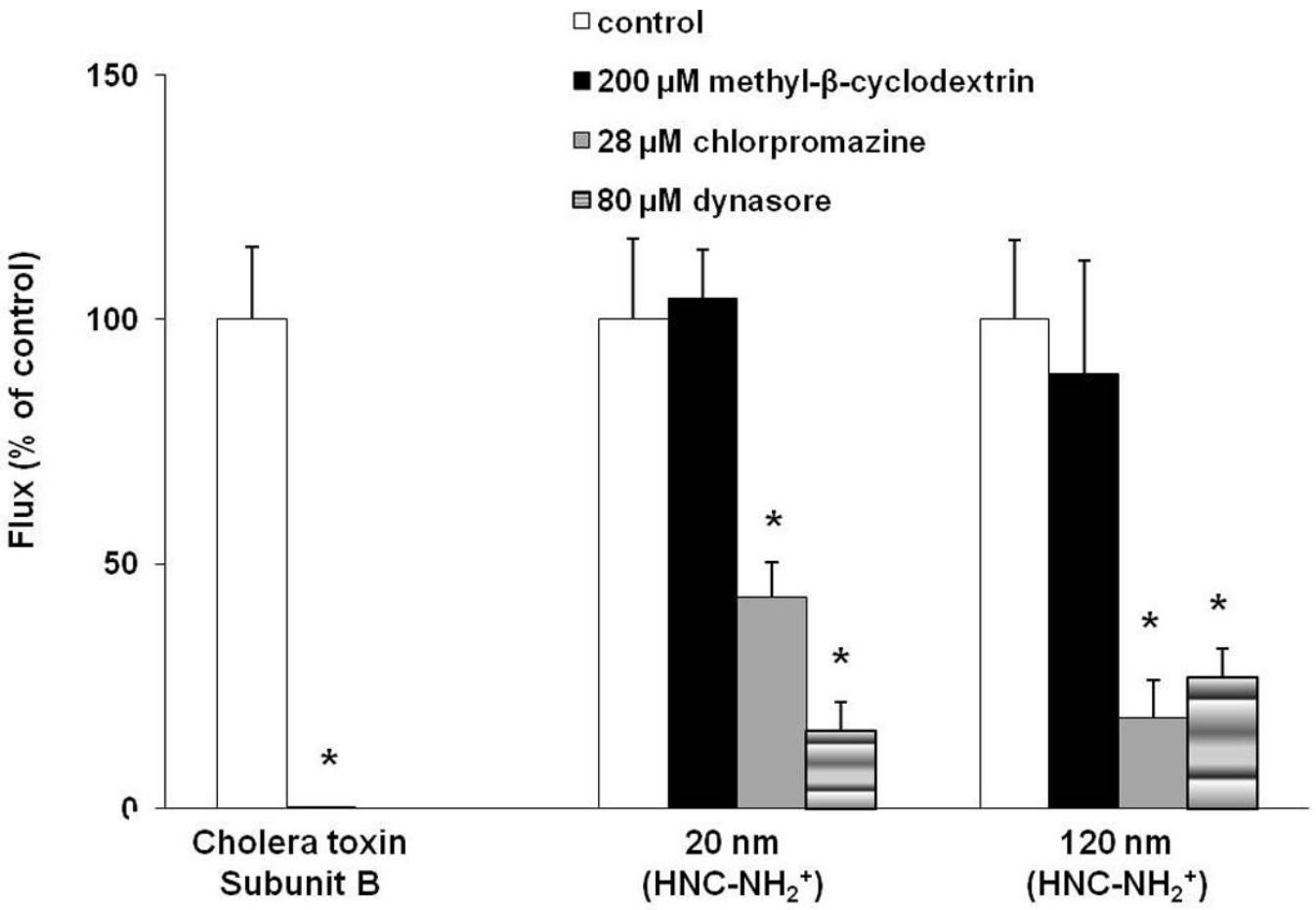

Figure 3.

Effects of inhibition of lipid raft-mediated, clathrin-mediated and dynamin-dependent endocytosis on flux of amidine-modified (positively charged, 20 and 120 nm) PNP across MAECM at 24 h. Apical [PNP] = 176 μg/mL. PNP flux across monolayers treated with 200 μM MBC did not decrease (n=3), while that across monolayers treated with either 28 μM chlorpromazine or 80 μM dynasore markedly decreased by 75% and 80%, respectively, compared to corresponding controls (n=5–6). Flux of cholera toxin subunit B (CTB, apical concentration of 50 μg/mL; n=6) was measured across MAECM as positive control for caveolin-mediated endocytosis, showing 98% inhibition in the presence of MBC. * = significantly different from respective control.

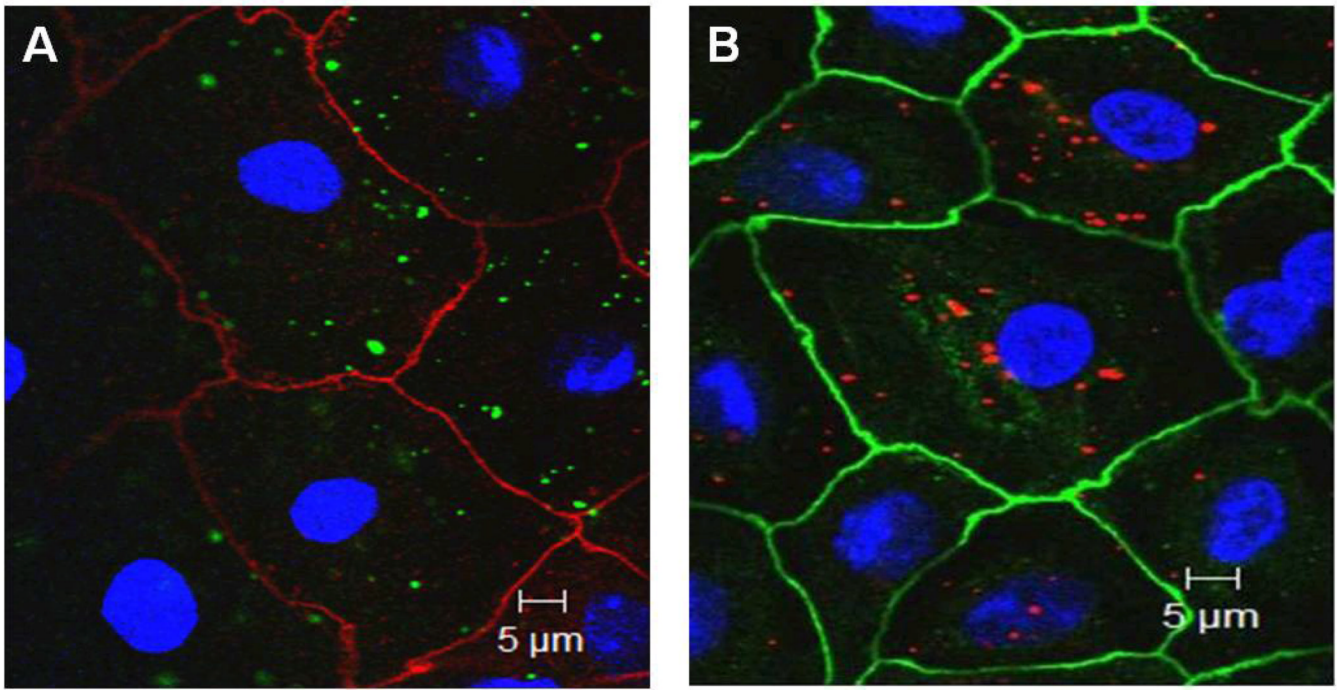

Figure 4.

Midsection confocal images of MAECM exposed at 37°C apically to (A) PNP (120 nm amidine-modified, positively charged) or (B) PNP (100 nm carboxylate-modified, negatively charged) at 176 μg/mL for 24 h. Cell borders are stained for ZO-1 (red in panel A and green in panel B), nuclei are stained by DAPI (blue) and PNP appear green in panel A and red in panel B. PNP are largely intracellular (i.e., not at cell-cell junctions or in nuclei).

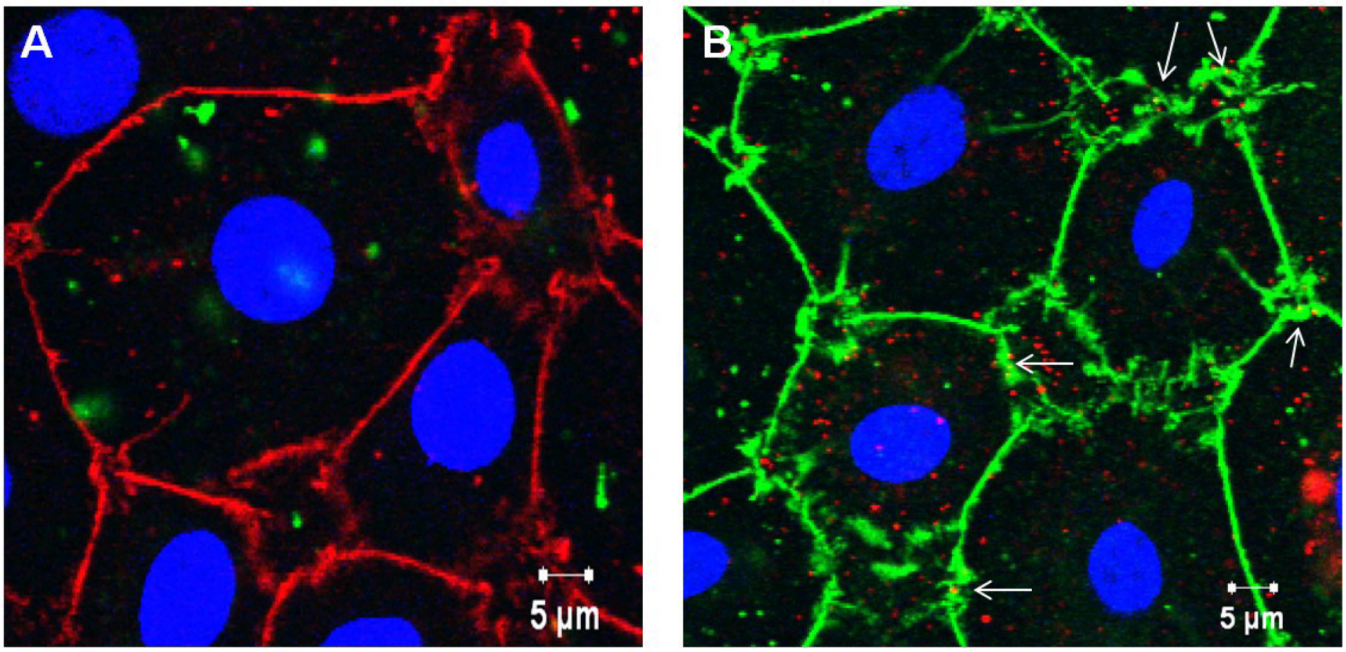

Figure 5.

Midsection confocal photomicrographs are shown for MAECM treated with 2 mM EGTA and exposed to apical [PNP] of 176 μg/mL (120 nm amidine-modified (positively charged) PNP in green in panel A or 100 nm carboxylate-modified (negatively charged) PNP in red in panel B) for 24 h. Cell-cell borders (ZO-1 staining) appear red and green in panels A and B, respectively, while nuclei are blue in both panels. In panel B, a few PNP may be seen in disrupted cell-cell borders (arrows).

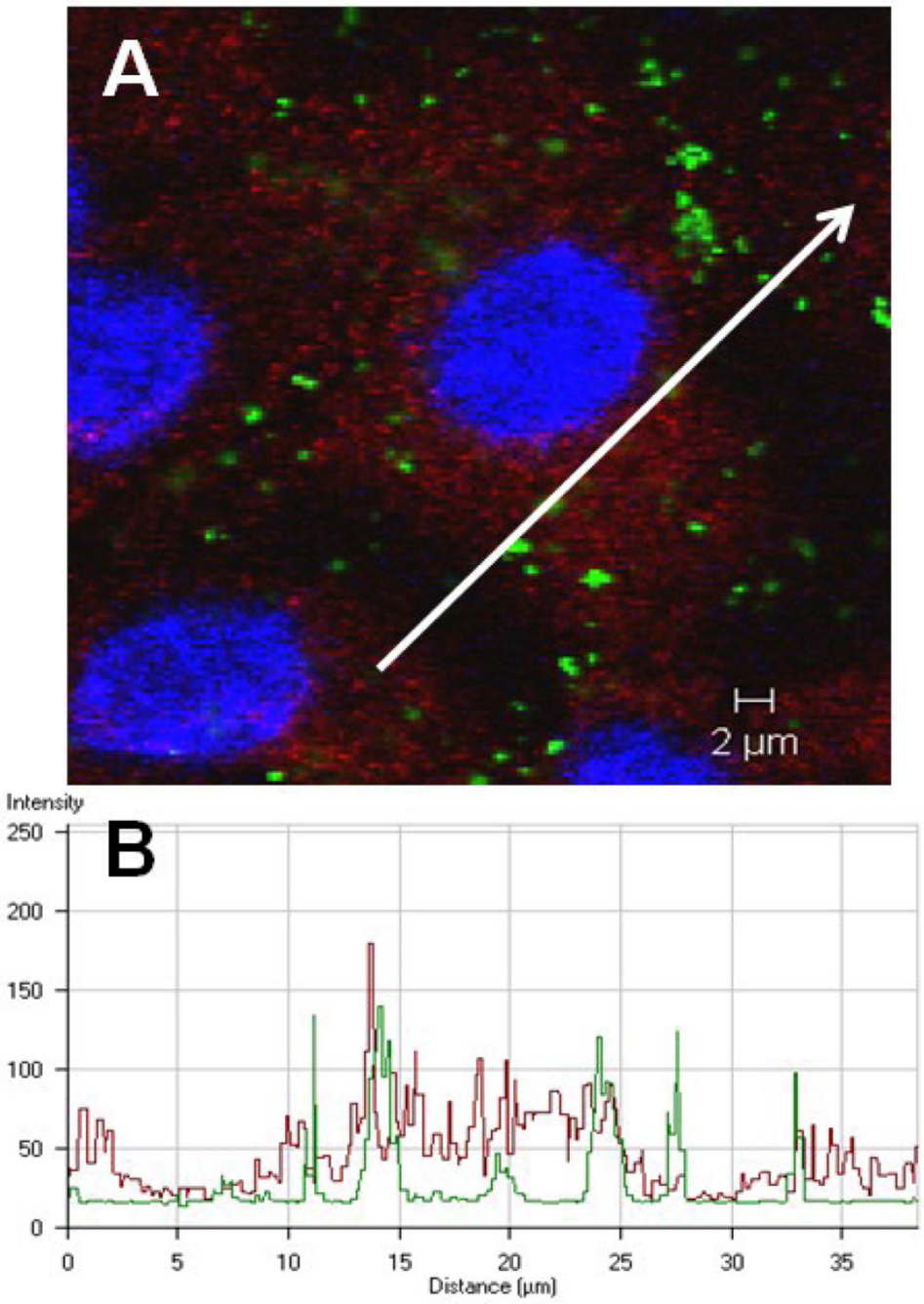

Figure 6.

Confocal photomicrograph showing internalized PNP (120 nm amidine-modified, positively charged)) and clathrin heavy chain in MAECM after 1 h of apical exposure to 176 µg/mL PNP. Nuclei are blue, clathrin heavy chain is red and PNP appear green (panel A). In panel B, association of color intensities for PNP (green) and clathrin heavy chain (red) is seen along the line segment depicted in panel A, representing an example of 11 different line graph analyses.